DETECTION OF THE ANGLE CHANGE BETWEEN CAMERA AND STAR TRACKER BASED ON STAR OBSERVATION

Guan Zhichao [1*], Zhang Guo [1], Jiang Yonghua [2], Zhong Xing [3], Deng Mingjun [4], Li Beibei [3], Zhang Hao [5]

[1] State Key Laboratory of Information Engineering in Surveying, Mapping and Remote Sensing (LIESMARS), Wuhan University, Wuhan 430079, China
[2] School of Remote Sensing and Information Engineering, Wuhan University, Wuhan 430079, China
[3] Chang Guang Satellite Technology CO, LTD, Jilin Changchun 130033, China
[4] School of Automation and Electronic Information, Xiangtan University, Xiangtan, 411105, China
[5] School of Geographic and Biologic Information, Nanjing University of Posts and Telecommunications, Nanjing, 210049, China

Commission I, WG I/4

KEY WORDS: Star observation, Star Tracker, Camera, Angle change, Jilin-1 satellite, Attitude error.

ABSTRACT:

Satellites in orbit are affected by changes in thermal environment and other factors, and the angle of optical axis between the camera and star tracker (Cam-ST) changes. As a result, the attitude measurement error of the orbital period appears, leading to a decrease in the accuracy of the geometric positioning of the image. This paper proposes a star observation mode, using the stars as the control point, so as to detect the angle change between the Cam-ST throughout the orbital period. This paper is based on 20 sets of star observation data from the Jilin-1 video satellite. Through methods such as star point extraction and pre-recognition, the camera's pointing in the inertial space is obtained. Then the angle with the optical axis of star tracker (ST) is calculated, and the error law of the angle between the Cam-ST is obtained. The experimental results show that the Cam-ST optical axis angle will produce a regular error change during the satellite orbit period. After fitting, the error of the angle between the camera and the star tracker (Cam-ST) is reduced from 47.86" to 5.63". Through the method of star observation, the errors between Cam-ST angle can be effectively improved. The high accuracy of the camera's pointing measurement within the orbit period range is of great significance for satellite global mapping without ground control points (GCPs).

1. INTRODUCTION

1.1 Changes Between Camera and Star Tracker

The ST is the main load of the satellite attitude measurement, and the accurate installation relationship between the Cam-ST is the key factor of the geometric positioning accuracy of the optical remote sensing satellite. After the satellite is in orbit, it is affected by the different cold and hot space environments, causing the angle of the optical axis between the Cam-ST to change, thereby reducing the geometric positioning accuracy of the satellite image. At present, scholars from various countries mainly use the ground high-precision control points to calibrate the Cam-ST angle of satellites. After calibration, the ALOS satellite launched by Japan in 2006 has a positioning accuracy of 8m, with an equivalent angle error of 2.4" (resolution 2.5m, orbital height 691km, sub-satellite point 1" error equals to 3.35m error) (Tadono et al., 2009; Takaku et al., 2009); The French SPOT 6/7 launched in 2012/2014, have a positioning accuracy of 7.8m with 2m resolution image, and the equivalent angle error is 2.3" (Amberg, et al., 2013). the US's Worldview-3/4 satellite launched in 2014/2016 have a 0.31m resolution image and the positioning accuracy can reach 2.7m, and the equivalent angle error is 0.9" (Hu et al., 2016; Bresnahan et al., 2015).

However, a single calibration cannot completely guarantee the global positioning accuracy of satellites. Through the calculation of multiple ST parameters measured in orbit, the orbital periodic change of the angle between the ST and ST can be found, which confirms that there is a change in the angle between the Cam-ST in the orbital period (Zhang et al., 2018). This phenomenon has been discovered on multiple satellites. For example, CHAMP satellite launched by Germany in 2000 was discovered that there is an angle error of up to 36" between the star trackers (STs) in one orbit data (Jørgensen et al., 2015). Comparing different orbits, it is found that the same phenomenon still exists. The PROBA satellite of European space agency (ESA) is affected by thermal deformation, and there is a change in the angle between the STs (Jørgensen et al., 2015). The China Tianhui-1 satellite launched in 2012 found the same angle change as the orbital period, and the maximum change of the angle was close to 30", it will have an impact of nearly 70m on the positioning accuracy (Wang et al., 2016). One of the high-resolution optical satellites launched by China in 2016, also have obvious angle changes on three STs that consistent with the orbital period (Wang et al., 2016).

For these reason, it is necessary to model the changes in the angle between the Cam-ST of the satellite, so as to eliminate the error. The Centre national d'études spatiales (CNES) of French has established 21 geometric calibration fields within the globe. It uses distributed calibration field to perform 5-degree polynomial fitting on the angle between the SPOT5's Cam-ST, and achieving accurate positioning (Breton et al., 2002; Valorge et al., 2004). The ALOS satellites updated the correction parameters multiple times to compensate for the relative installation error between the Cam-STs (Iwata., 2010). In order to overcome the dependence on control points, satellite Pléiades' use the agile ability to implement an Auto-Calibration mode in imaging, which can calibrate the Cam-ST's angle error (Greslou et al., 2012; Fourest et al., 2012). However, the existing calibration methods using

* Corresponding author

GCPs are limited by the acquisition difficulty of control data, and it is difficult to achieve high-frequency calibration; while the Auto-Calibration method like Pléiades does not rely on control data, but it requires satellites to have strong agility and mobility, poor applicability for normal optical satellite.

1.2 Star Observation Idea

Since the coordinates of the star in the celestial coordinate system are determined, and its position calculation accuracy is better than 0.1", it is a very ideal control point source. The calibration parameters obtained through star observation are not essentially different from those obtained through GCPs calibration (Guan et al., 2019). Under reasonable imaging planning conditions, for example, through slow attitude maneuver, it is feasible to use the camera to image the star (Greslou et al., 2012). Meanwhile, the array camera can take pictures of stars through long-time exposure. Therefore, it's operationality for most of the satellite missions with video or array camera.

Jilin-1 07 video satellite was launched on January 19, 2018. After being in orbit, its positioning accuracy is unstable due to the angle change between the Cam-ST. This manuscript will use the ability of deep space imaging of Jilin-1 07 video satellite, use the camera to photograph the stars at different position in one orbit (as shown in the Figure 1 below). By converting the star's right ascension and declination information into pointing information, the camera's pointing is obtained. Then the angle change detection between the Cam-ST within one orbital period can be achieved. Because the gyro measures the relative change of satellite attitude and is not sensitive to the change of angle, the gyro data will not be used in this paper.

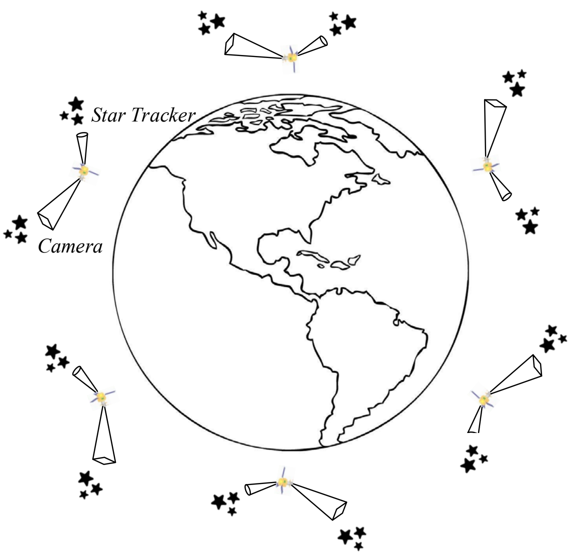

Figure 1. Camera photograph the stars at different position in one orbit.

The processing flowchart of the star observation data is as follows. First, process the star image obtained by the camera, and obtain star point information through star point extraction and star point recognition based on a priori attitude. Then the optical axis direction of the camera is obtained, and the optical axis of the ST's direction is obtained according to the attitude information measured by ST. Finally, through angle calculation between Cam-ST, the angle change is obtained.

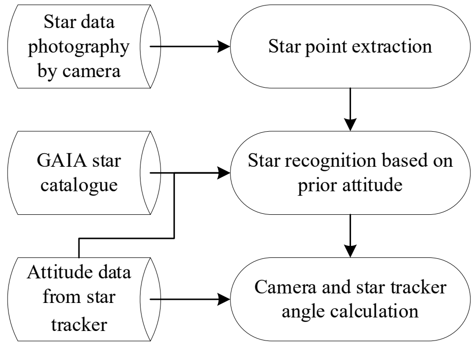

Figure 2. Processing flowchart of the star observation data.

2. METHOD

2.1 Star Points Coordinate Extraction

When the camera shoots the starry sky, the background is black. But the camera has a certain noise floor due to factors such as sensor current. It needs to be segmented by the background threshold method to separate the star points and the background in the image. Assuming that the digital number (DN) value of the image containing the star points is expressed as $g(x, y)$, and t is the background threshold, the image binarization is:

$$f(x,y) = \begin{cases} 1, & g(x,y) \geq t \\ 0, & g(x,y) < t \end{cases}, \tag{1}$$

Since this experiment involves star observations at different orbital positions, the image will inevitably be affected by sunlight at some imaging angles. Therefore, the threshold is selected as a fixed value within a period of time and will not be unique in different periods of time.

The part of $f(x, y)$ with a value of 1 is marked by the connected domain algorithm, and k groups of connected domains $\Omega_i, i = \{1,2, \dots k\}$ are obtained. Each group of connected domains is composed of different numbers and adjacent pixels, and:

$$\forall \Omega_{i \in C} \cap \forall \Omega_{j \in C} = 0, i \neq j, C = \{1,2, \dots, k\}, \tag{2}$$

The connected domain formed by the star points is shown as a round shape. In order to improve the accuracy of star point extraction and avoid the influence of cosmic high-energy ray particles and sun stray light, by calculating the round rate of the star point and selecting a star point with a higher round rate, real stars can be further filtered out. The round rate calculation formula is as follows:

$$P = \frac{4\pi S}{L^2}, \tag{3}$$

among them, P represents the round rate, S represents the area of the connected domain, and L represents the perimeter of the connected domain. From the relationship between the circular area and the perimeter, it can be seen that the closer P is to 1, the more circular the connected domain is. Usually, the round rate of the star point is greater than 0.6.

When the star points are filtered out, the centre coordinates of the star can be extracted by the centroid method, and the centroid sub-pixel coordinates $(\bar{x}, \bar{y})$ of the star can be obtained by the gray square weighted centroid method. The calculation formula is:

https://doi.org/10.5194/isprs-annals-V-1-2022-77-2022

$$\begin{cases} \bar{x} = \sum_{(x,y)\in\Omega} x \cdot g(x,y)^2 / \sum_{(x,y)\in\Omega} g(x,y)^2 \\ \bar{y} = \sum_{(x,y)\in\Omega} y \cdot g(x,y)^2 / \sum_{(x,y)\in\Omega} g(x,y)^2 \end{cases}, \tag{4}$$

2.2 Star Point Recognition Based on Prior Attitude

Generally, in order to obtain more information about stars, the field of view of the ST is relatively large, while the field of view of the camera mounted on the satellite is very small. It is more difficult to perform star recognition directly based on the extracted star points. Considering that although the angle between Cam-ST has changed, it is still a small change. Therefore, in the star recognition part, the known ST measurement value and the installation relationship between Cam-ST can be used.

According to the small hole imaging model, there should be a one-to-one correspondence between the observed star vector obtained by the camera and the star catalogue vector. The ascension and declination of the i-th star in the instantaneous J2000 coordinate system are (α_i, δ_i), which can be expressed as the azimuth vector $\boldsymbol{Z}_i$:

$$\boldsymbol{Z}_i = \begin{bmatrix} cos\alpha_i cos\delta_i \\ sin\alpha_i cos\delta_i \\ sin\delta_i \end{bmatrix}. \tag{5}$$

When the i-th star is photographed, the attitude matrix of the camera in the J2000 coordinate system measured by ST is $\boldsymbol{R}_{J2000}^{Cam}$, then the relationship between the vector $\boldsymbol{W}_i$ (the i-th star in the camera coordinate system) and $\boldsymbol{Z}_i$ is:

$$\boldsymbol{W}_i = \boldsymbol{R}_{J2000}^{Cam} \boldsymbol{Z}_i. \tag{6}$$

After imaging by the camera, the coordinates of the i-th star on the image are (x_i, y_i), then the relationship between $\boldsymbol{W}_i$ and the coordinates of the image point is:

$$\boldsymbol{W}_i = \begin{bmatrix} W_{i1} \\ W_{i2} \\ W_{i3} \end{bmatrix} = \frac{1}{\sqrt{((x_i - x_0)^2 + (y_i - y_0)^2 + f^2)}} \begin{bmatrix} x_i - x_0 \\ y_i - y_0 \\ -f \end{bmatrix}, \tag{7}$$

among them, f is the main distance of the optical lens of the camera, and (x_0, y_0) is the intersection of the optical axis of the camera and the image plane. According to the above formula, the calculation formula for the coordinates of the i-th star can be obtained as:

$$\begin{cases} x_i = x_0 - \frac{W_{i1}}{W_{i3}} * f \\ y_i = y_0 - \frac{W_{i2}}{W_{i3}} * f \end{cases}. \tag{8}$$

Bring all the stars from the GAIA star catalogue (AreNou et al., 2018) into formula (5), according to the ST measurement attitude into formula (6), and then use formulas (7) and (8) to get the image point coordinates. If the calculated image point coordinates are in the image, it is compared with the extracted neighbouring stars. Within a certain threshold range, the pairing is considered successful. Then the corresponding relationship between the star point coordinates in image and the right ascension/declination of stars in the J2000 system is established.

2.3 Cam-ST Angle Calculation Algorithm

Figure 3 shows the relationship between camera coordinate system $O - XYZ_{Cam}$, star sensor coordinate system $O - XYZ_{ST}$ and inertial coordinate system $O - XYZ_{J2000}$. The camera photograph stars to obtain its pointing information $\boldsymbol{V}_{J2000}^{Cam}$. Star sensors photograph stars to obtain its pointing information $\boldsymbol{V}_{J2000}^{Star}$. The Cam-ST angle means the angle between $\boldsymbol{V}_{J2000}^{Cam}$ and $\boldsymbol{V}_{J2000}^{Star}$.

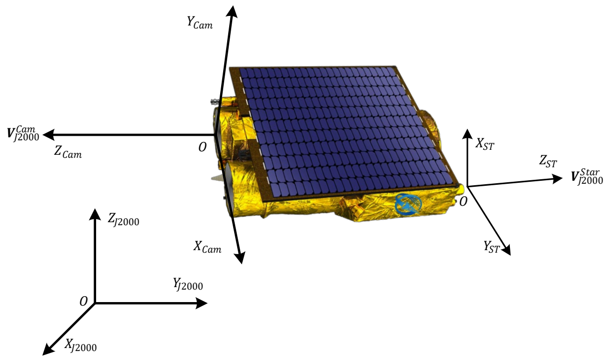

Figure 3. The relationship between camera coordinate system, star sensor coordinate system and inertial coordinate system.

Only two stars are needed to determine the camera's attitude estimation under the J2000 series. Usually, multiple stars are recognized in the camera or ST's field of view. At this time, multiple stars have established redundant observations. The problem of determining the satellite's three-axis attitude can be equivalent to the Wahba problem, which is to find the optimal attitude based on the least squares criterion:

$$J(\widehat{\boldsymbol{R}}_{J2000}^{Cam}) = \frac{1}{2}\sum_{i=0}^{n} a_i \left\| \boldsymbol{W}_i - \widehat{\boldsymbol{R}}_{J2000}^{Cam} \boldsymbol{Z}_i \right\|^2, \tag{9}$$

among them, $a_i \geq 0$ is the weighting factor. The camera pose matrix $\widehat{\boldsymbol{R}}_{J2000}^{Cam}$ can be obtained through the q-Method algorithm (Markley and Crassidis., 2014). Because the X/Y axis accuracy of the ST is higher than that of the Z axis, the direct detection of the angle between the optical axis of the Cam-ST can accurately reflect the change of the installation matrix between the Cam-ST. Assuming that the attitude of ST in the J2000 system is $\widehat{\boldsymbol{R}}_{J2000}^{Star}$, according to the following method to obtain the pointing directions of the camera and ST in the J2000 coordinate system, respectively:

$$\begin{cases} \boldsymbol{V}_{J2000}^{Star} = \widehat{\boldsymbol{R}}_{J2000}^{Star} \boldsymbol{Opt} \\ \boldsymbol{V}_{J2000}^{Cam} = \widehat{\boldsymbol{R}}_{J2000}^{Cam} \boldsymbol{Opt} \end{cases}, \tag{10}$$

and

$$\boldsymbol{Opt} = [\boldsymbol{0}, \boldsymbol{0}, \boldsymbol{1}]. \tag{11}$$

Then the formula for calculating the angle θ between the Cam-ST is

$$\theta = arccos\left(\frac{\boldsymbol{V}_{J2000}^{Star} \cdot \boldsymbol{V}_{J2000}^{Cam}}{|\boldsymbol{V}_{J2000}^{Star}| \cdot |\boldsymbol{V}_{J2000}^{Cam}|}\right). \tag{12}$$

3. EXPERIMENTAL DATA

3.1 Jilin-1 Data Introduction

In this study, the array camera of Jilin-1 07 video satellite was used to conduct experiments and verification of star observation. The following table shows the relevant parameters of the Jilin-1 07 video satellite's Cam-ST.

https://doi.org/10.5194/isprs-annals-V-1-2022-77-2022

Jilin-1 07 Satellite	Launch Date	Jan. 19th 2018
Camera parameters	Image resolution	0.92m (Nadir)
	Pixel numbers	12000 (length) 5000 (width)
	Focal length	3.2 m
	Pixel size	5.5 μ
	Field view	70.5′× 29.4′
	Angular resolution	0.352″
	Exposure period	2/5 Hz
	Exposure duration	450 ms /200 ms
Star Tracker parameters	Triaxial error	X/Y: 7″, Z: 30″
	Frequency	2 Hz

Table 1. The introduction of Cam-ST of Jilin-1 video satellite.

There are two satellite star observation tasks, which were taken on October 26th and November 13th, 2020. The video camera is taken in a circle of orbit, with a time interval of 10 minutes and a latitude of approximately 36°. The camera works 10 times in each task, each time the camera is aimed at the same stellar area. Satellites keep their attitude unchanging in the inertial system when imaging stars. Among them, the camera of task 101~110 shoots for 6s each time, and exposes for 200ms per video frame. The camera of task 201~210 shoots for 12s each time, and exposes for 450ms per video frame.

The following Table 2 shows the time, latitude and longitude of the 20 tasks of star observation, as well as the availability of the Cam-ST. A table with a darker color, such as several tasks id 101, 107, 108, 109, and 110, are represented as imaging in the shadow area, while a table with no color represents the imaging in the illuminated area. It can be seen from the table that in the shadow area, the Cam-ST can output parameters normally in most cases because they are not affected by the sun. In the illuminated area, due to the relationship with the angle of the sun, sometimes the camera cannot obtain a valid image, and sometimes the ST parameter cannot be output.

The star catalogue data used in this experiment is the GAIA EDR2 catalogue data published in April 2018, which contains the measurement parameters of 1.69 billion celestial bodies. The original GAIA star catalogue data contains the highest 21 magnitude stars, and the data volume is about 1.26TB. Jilin-1 can photograph stars of magnitude 13 and the minimum number of stars required to establish a camera pointing is 2. Considering the processing time, this experiment selects stars with magnitude less than 11 in the GAIA catalogue as the pointing control point. The experimental star catalogue contains about 1.24 million celestial bodies.

Imaging Time			Imaging Position		Data available	
Date	Task ID	Time UTC +8	Latitude	Longitude	Camera	Star Tracker
Oct. 26th,2020	101	06:10:30	75	-154	Yes	Yes
	102	06:20:30	39	179	—	Yes
	103	06:30:30	1	171	Yes	Yes
	104	06:40:30	-36	162	Yes	Yes
	105	06:50:30	-72	141	Yes	Yes
	106	07:00:30	-67	1	Yes	Yes
	107	07:10:30	-30	-14	Yes	Yes
	108	07:20:30	7	-22	Yes	Yes
	109	07:30:30	44	-31	Yes	Yes
	110	07:40:30	79	-72	Yes	
Nov. 13th,2020	201	05:06:00	82	-91	Yes	Yes
	202	05:16:00	50	-161	Yes	—
	203	05:26:00	12	-171	Yes	—
	204	05:36:00	-25	-179	Yes	Yes
	205	05:46:00	-61	167	Yes	—
	206	05:56:00	-78	35	Yes	Yes
	207	06:06:00	-42	2	Yes	Yes
	208	06:16:00	-4	-5	Yes	Yes
	209	06:26:00	33	-13	Yes	Yes
	210	06:36:00	70	-32	Yes	Yes

Table 2. Imaging time and status of star observation of Jilin-1 video satellite.

4. EXPERIMENTAL RESULT AND ANALYSIS

There are a total of 20 sets of data in this study, among which the 10 sets of data in Oct 26th will be used as the angle model construction data, and the 10 sets of data in Nov. 13th will be used as the model accuracy verification data. This article will analyse the changes in the orbital period of the Cam-ST angle error, the angle rule and the compensation result.

4.1 Angle Measurement Error

As shown in the Figure 4, it is the measured angle of the Cam-ST in one set of data. Figure 4(a) is the angle between the Cam-ST in task 108, with an average value of about 119.2792°. Within the 6 seconds imaging time, the measurement error of the Cam-ST's angle is about ±4", which is in line with the error design of the ST. Figure 4(b) shows the angle between the Cam-ST in task 208. The average value is also 119.2792°, and the measurement error is about ±2.5″. For other tasks, the measurement errors are all within the design range of the ST of ±7″ (as shown in Table 1). This shows that the angle detection between the Cam-ST is mainly affected by the measurement error of the ST. Through follow-up analysis shows that the error does not affect the detection of the angle change between the Cam-ST.

https://doi.org/10.5194/isprs-annals-V-1-2022-77-2022 | © Author(s) 2022. CC BY 4.0 License.

4.2 Cam-ST Angle Change Detection

After obtaining all valid data, the Cam-ST angle changes of the 20 tasks are shown in the Figure 5 below. The abscissa represents the variation range of latitude, and the ordinate represents the residual error of the measured angle minus the average value. The circle represents the residual angle of tasks 101~110 at different times, and the triangle represents the residual angle of tasks 201~210 at different times. Since each imaging time is less than 12s, the change in the latitude of the satellite's flight distance is relatively short, so the points gathered together vertically in the Figure 5 represent the residual angle of one task. The vertical width of each group of points together represents the measurement error of the angle of the Cam-ST. Since imaging in the shadow area is less affected by sun light, the effective value of the camera or ST is more. In the illuminated area, the camera or ST sometimes cannot obtain valid data. At this time, the angle data between the Cam-ST will be missing.

It can be seen from Figure 5 that the angle between the Cam-ST increases with the increase in latitude, and the change of the angle has obvious regularity. The change trend is the same for the two imaging dates. As Figure 5 shown, the angles change of Cam-ST are ±25" within north-south latitude. For several imaging analyses on date October 26th, the following rules can be found. In the first star observation task 101, the satellite had just passed the northernmost end of the orbit. At this time, the satellite is still in the shadow area, and the angle between the Cam-ST is the largest. As the latitude decreases, the angle between the Cam-ST decreases as task 103 shown. And as task 104 and 105 shown, the latitude continue to decrease, the angle between the Cam-ST gradually decreases. When the satellite re-enters the shadow area as task 106 shown, the angle between the Cam-ST reaches the minimum. As the latitude of the satellite increases, for example, the latitudes of tasks 107, 108, and 109 gradually increase, and the angle between Cam-ST gradually returns to the initial size. It should be noted that the angle detection data obtained by imaging in the illuminated area is relatively small and unstable, but it is still consistent with the overall angle change trend. For several imaging on November 13th, the patterns are similar. Special attention should be paid to the task 204. This set of data is the only valid measurement data for the illuminated area in that day. But from the perspective of the change trend, it is still consistent with the change in the shadow area.

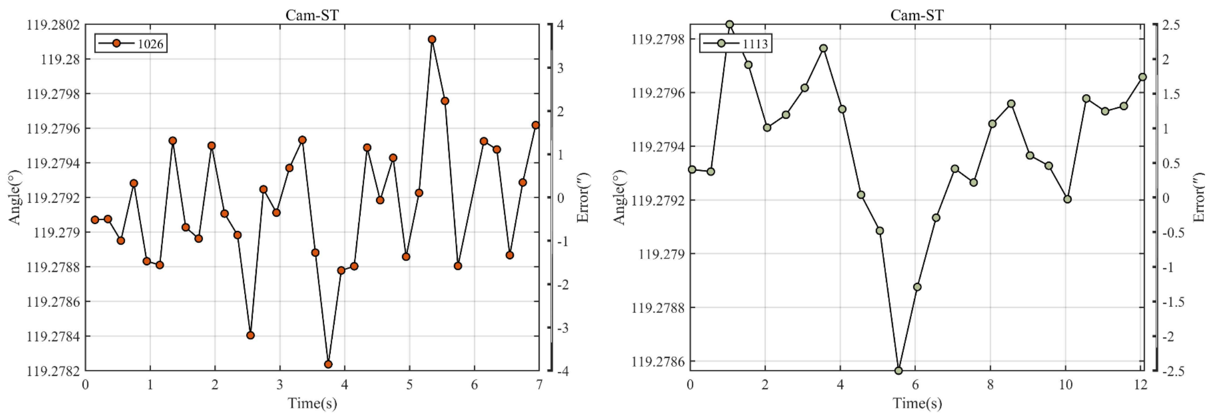

(a) task 108 (b) task 208

Figure 4. Angle measurement error of Cam-ST.

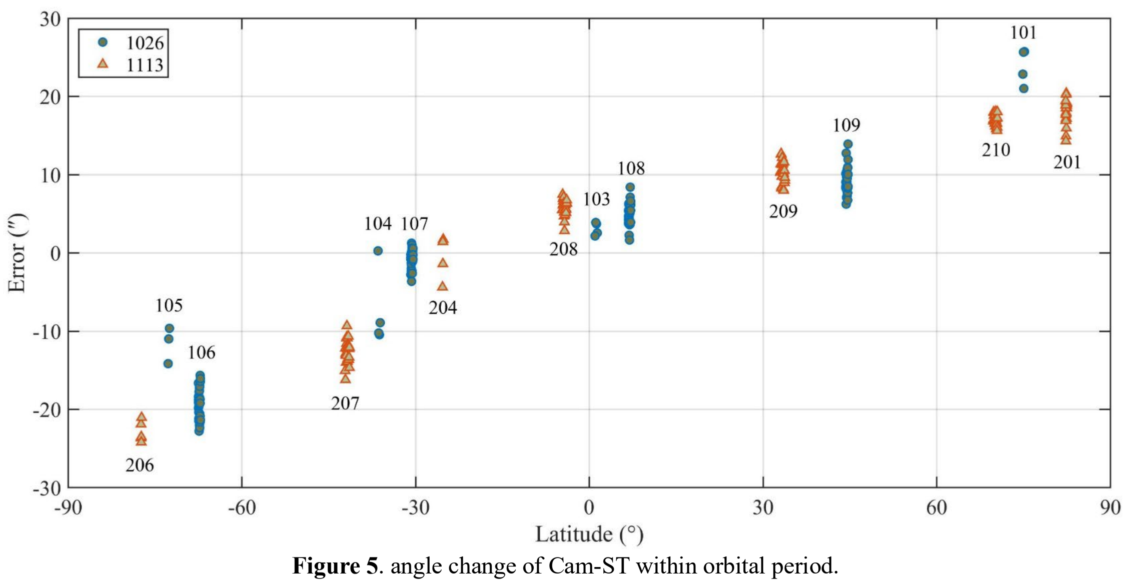

Figure 5. angle change of Cam-ST within orbital period.

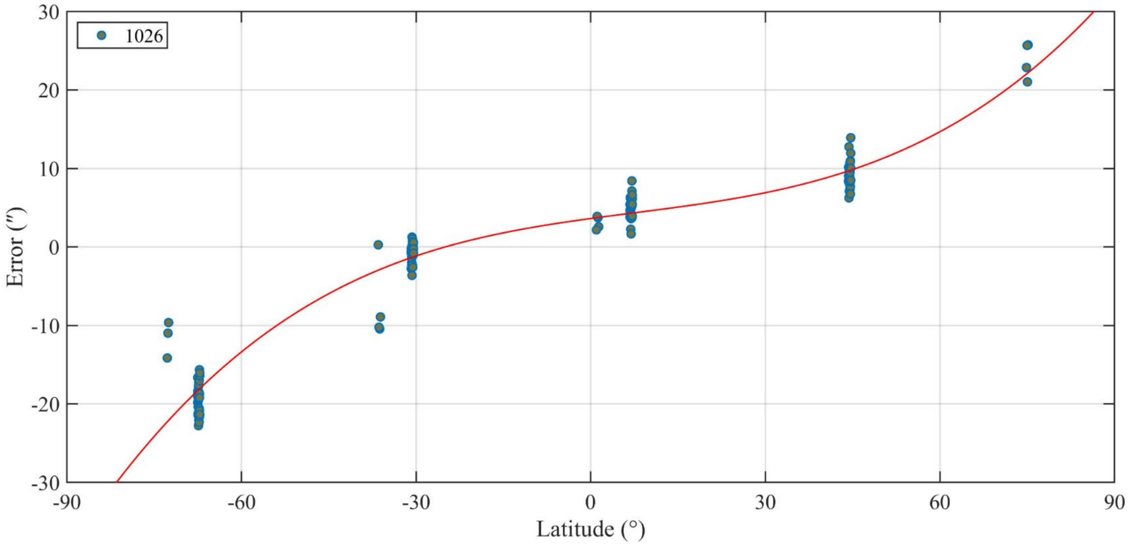

Figure 6. Angle change fitting of Cam-ST based on task 101~109.

4.3 Fitting Analysis

Since the angles of two tasks between Cam-ST have high regularity in latitude. We can use one part of the tasks to establish the angle change model, and use the other part of the tasks as accuracy verification. The Figure 6 show the fitting curve of the angle change of the Cam-ST based on task 101~109. Then task 201~210 would be used as verification. Among them, the angle change of the Cam-ST can be fitted with a third-degree polynomial.

The residual error of the angle after fitting is counted, and the results are shown in the following Table 3. It counts the effective Cam-ST angle fitting residual data in the 15 tasks, and calculates the maximum and minimum errors and the root mean square (RMS) error in each group of arrays.

Date	Task ID	Cam-ST Angle Error Before Fitting (arcsecond)			Cam-ST Angle Error After Fitting (arcsecond)		
		MIN	MAX	RMS	MIN	MAX	RMS
Oct. 26th,2020	101	-0.66	3.98	2.32	-0.84	-3.59	2.62
	103	21.12	22.83	21.93	0.01	1.53	0.97
	104	24.73	35.44	32.63	-3.24	7.54	6.27
	105	34.64	39.15	36.64	-8.14	-12.47	10.76
	106	40.65	47.77	44.27	0.07	4.54	2.15
	107	23.75	28.63	25.91	0.06	-2.60	1.23
	108	16.59	23.35	20.1	-0.00	-4.12	1.51
	109	11.09	18.76	15.96	-0.02	-4.15	1.77
	RMS Total	2.32	**44.27**	28.32	0.97	10.76	**2.49**
Nov. 13th,2020	201	4.6	10.69	7.12	6.52	12.56	9.00
	204	23.27	29.38	25.77	1.31	4.28	2.53
	206	46.04	49.19	47.86	-2.03	-5.13	3.58
	207	34.33	41.2	37.57	4.54	11.33	7.93
	208	17.53	22.17	19.22	0.32	-4.36	2.84
	209	12.33	17.02	14.67	-0.52	-5.29	3.24
	210	6.92	9.38	8.02	1.17	3.87	2.45
	RMS Total	7.12	**47.86**	22.42	2.45	9.00	**5.63**

Table 3. Cam-ST angle error before and after fitting

Before the correction of the angle between the Cam-ST, task 101 is used as the calibration time for the angle between the Cam-ST. After calibration, the error of the angle between the Cam-ST is 2.32" for task 101. However, as the satellite imaging latitude gradually decreases, the error of the angle will become larger and larger after using this parameter in other tasks. At the time of task 106, the angle difference is the largest, and the RMS error can reach 44.27". Bringing the same Cam-ST angle parameters into tasks 201~210, it can be found that the angle error is the largest at task 206, and the RMS error can reach 47.86". If the orbital period model of Cam-ST is not performed, such an angle error between the Cam-ST will have a greater impact on the accuracy of geometric positioning.

For tasks 101~109 after fitting, the minimum value of the total residual error after fitting is 0.97", the maximum is 10.76", and the median error is 2.49". The error caused by Cam-ST angle change will effectively compensate. In general for tasks 101~109, the RMS error is reduced from 44.27" before fitting to 2.49". Since this set of data with task 105 is daytime imaging, And the imaging position is near the equator, the Cam-ST are affected by relatively strong sunlight at this time, causing the angle change to be slightly offset from the fitting curve. The fitting model of the angle change between Cam-ST was brought into tasks 201~210 to verify the accuracy of the model. The results show that, the minimum value of the total residual error after fitting is 2.45", the maximum is 9.00", and the median error is 5.63". In general for tasks 201~210, the RMS error is reduced from 47.86" before compensation to 5.63".

The two accuracy verification results show that the use of star observations in the full orbital period can effectively establish a model of the change in the angle between the Cam-ST's optical axis. This model can be used in subsequent earth observation tasks to reduce the geometric positioning error caused by the change in the angle between Cam-ST.

5. CONCLUSIONS

Camera star observation is an effective method for detecting the angle between the Cam-ST. With this method, the model of the angle change between the Cam-ST can be constructed for the entire orbit without a global GCP. Using this change model, the subsequent change error of the Cam-ST can be effectively eliminated. In this paper, the detection results of 20 sets of star observation data used in the 20 tasks of the Jilin-1 07 video star show that the angle change model is established, and the error of the Cam-ST's angle can be reduced from 47.86" to 5.63". This method effectively improves the pointing accuracy of the camera and provides a better guarantee for the subsequent improvement of geometric accuracy. In the next work, we will take more data to establish the change model of Cam-ST's angle, and compare it with the accuracy verified by GCP.

ACKNOWLEDGEMENTS

This work has made use of data from the European Space Agency (ESA) mission Gaia (https://www.cosmos.esa.int/gaia), processed by the Gaia Data Processing and Analysis Consortium DPAC, https://www.cosmos.esa.int/web/gaia/dpac/consortium). Funding for the DPAC has been provided by national institutions, in particular the institutions participating in the Gaia Multilateral Agreement. This work supported by Key research and development program of the national (2020YFA0713503), Nature Science Foundation of Hunan Province Grant (2020JJ5537), Research Foundation of Education Department of Hunan Province Grant (19C1769)

REFERENCES

Amberg V., Dechoz C., Bernard L., et al., 2013. In-flight attitude perturbances estimation – Application to PLEIADES-HR satellites, *Proc Spie*. 8866, 206-209. doi.org/10.1117/12.2023275

AreNou F, Luri X, Babusiaux C, et al., 2018. Gaia data release 2: Catalogue validation. *Astronomy & Astrophysics*, 616 (A17):29-59. doi.org/10.1051/0004-6361/201833234

Bresnahan P., Brown E., Henry V. L., 2015: WorldView-3 Absolute Geolocation Accuracy Evaluation, *in Joint Agency Commercial Imagery Evaluation Workshop*.

Breton E, Bouillon A, Gachet R, et al., 2002. Pre-flight and in-flight geometric calibration of SPOT 5 HRG and HRS images.

Fourest S., Kubik P., Lebègue L. et al., 2012: Star-Based method for Pleiades HR Commissioning, *ISPRS - International Archives of the Photogrammetry, Remote Sensing and Spatial Information Sciences*, XXXIX-B1. 531-536, 0007-01-07.

Greslou D., Lussy F. D., Delvit J. M., et al., 2012: Pleiades-HR innovative techniques for geometric image quality commissioning. *ISPRS-International Archives of the Photogrammetry, Remote Sensing and Spatial Information Sciences*, XXXIX-B1:543-547.

Guan Z. C., Jiang Y. H., et al., 2019. Star-Based Calibration of the Installation Between the Camera and Star Sensor of the Luojia 1-01 Satellite. *Remote Sensing*, 11(18):2081. doi.org/10.3390/rs11182081

Hu F., Gao X. M., Li G. Y., et al., 2016: Dem Extraction from WORLDVIEW-3 Stereo-Images and Accuracy Evaluation, *International Archives of the Photogrammetry, Remote Sensing & Spatial Information Sciences*, XLI-B1, 327-332. doi.org/10.5194/isprsarchives-XLI-B1-327-2016

Iwata T., 2010: Ground-Based Precision Attitude Determination Using Repeated Smoothing with Sequential Rate Bias and Attitude Estimation. *AIAA Guidance, Navigation, and Control Conference*. doi.org/10.2514/6.2010-8451

Jørgensen J. L., Denver T., Betto M., et al., 2005. The PROBA satellite star tracker performance. *Acta Astronautica*, 56(1–2): 153-159. doi.org/10.1016/j.actaastro.2004.09.011

Jørgensen P. S., Jørgensen J. L., Denver T., et al., 2005. In-flight quality and accuracy of attitude measurements from the CHAMP advanced stellar compass. *Acta Astronautica*, 56(1–2): 181-186. doi.org/10.1016/j.actaastro.2004.09.012

Markley, F.L.; Crassidis, J.L., 2014. Fundamentals of Spacecraft Attitude Determination and Control. *Springer Science and Business Media LLC: Berlin/Heidelberg, Germany*. doi.org/10.1109/MCS.2015.2427046

Tadono T., Shimada M., Murakami H., et al., 2009. Calibration of PRISM and AVNIR-2 Onboard ALOS "Daichi", *IEEE Transactions on Geoscience & Remote Sensing*, 47, 4042-4050. doi.org/10.1109/IGARSS.2012.6352481

Takaku J. and Tadono, T., 2009. PRISM On-Orbit Geometric Calibration and DSM Performance, *IEEE Transactions on Geoscience & Remote Sensing*, 47, 4060-4073. doi.org/10.1109/TGRS.2009.2021649

Valorge C, Meygret A, Lebegue L, et al., 2004. Forty years of experience with SPOT in-flight calibration.

Wang M., Fang, C., Bo, Y., Cheng, Y., 2016: Low frequency error analysis and calibration for high-resolution optical satellite's uncontrolled geometric positioning. *International Archives of the Photogrammetry, Remote Sensing & Spatial Information Sciences*, 41. doi.org/10.5194/isprsarchives-XLI-B1-395-2016

Wang R. X., Wang J. R., Hu X., 2016. Low-frequency errors Compensation of Attitude Determination System in Satellite Photogrammetry. *Acta Geodaetica et Cartographica Sinica*, 45(02): 127-130. doi.org/10.11947/j.AGCS.2016.20150167

Zhang G., Guan Z. C., 2018. Primary Research on Reliability of Satellite Imaging Quality. *Geomatics and Information Science of Wuhan University*, 43, 1954. doi.org/10.13203/j.whugis20180202